Supplementary Data

Table of Contents

Supplementary Methods

Genetic analysis

Genomic DNA was extracted from whole blood and analyzed with next generation sequencing (NGS) technology. To this end, coding exons and exon-intron border regions of *BSND*, *CASR*, *CLCNKA*, *CLCNKB*, *CLDN10*, *CTNS*, *GNA11*, *KCNJ1*, *MAGED2*, *SLC12A1*, and *SLC12A3* genes were enriched (NimbleGen, Roche, USA) and subjected to parallel sequencing on an Illumina HiSeq1500 system (Illumina, USA) with a coverage of at least 20-fold. Sanger sequencing was performed in those DNA regions that cannot reliably be analyzed due to limitations inherent to target enrichment and NGS techniques. Deletions and duplications in *CASR*, *CLCNKB*, and *SLC12A3* genes were not detected by multiplex ligation-dependent probe amplification (SALSA MLPA probemixes P177, P266, P136, MRC-Holland, Netherlands). Bioinformatic analysis of NGS data was performed as previously described.[1] Variants with a minor allele frequency <1% were analyzed for potential pathogenicity. The reference genome assembly used was GRCh37/hg19 (UCSC Genome Browser). The homozygous *CLDN10* variant reported here was confirmed by polymerase chain reaction amplification and subsequent Sanger sequencing. Copy number variation analysis did not suggest hemizygosity. The *CLDN10* gene sequence referred to in this article is NM_006984.4.

Diuretics responsiveness testing

Diuretics responsiveness testing was based upon a previously published protocol.[2] Interfering medication regimes, if any, were stopped 7 days prior to testing. Yet, KCl supplementation, if installed, was continued. Tests were performed in the morning after an overnight fast in an outpatient setting. Subjects were asked to maintain a recumbent position during the entire test except for the voiding procedures. At t=0 min, subjects drank tap water at 4 ml/kg and intravenous Ringer's acetate was initiated at 2 ml/(kg·h) to ensure sufficient urine production. Baseline urine and venous blood samples were collected at t=30 min and t=60 min. Subsequently, either hydrochlorothiazide (50 mg orally) or furosemide (20 mg intravenously)[3,4] were administered. Urine and venous blood samples were collected every 30 minutes until t=240 min. In the patient, a

washout period of 7 days was required to pass between both diuretics tests. For the determination of fractional excretions of monovalent ions, total serum electrolyte concentrations were used. For fractional excretions of divalent cations, total serum Mg^{2+} levels multiplied by a correction factor[5] of 0.7 and ionized Ca^{2+} levels from venous blood gas analyses were used, respectively.

Water deprivation and hypertonic saline infusion tests

Water deprivation tests were essentially performed as previously described.[6] The first test was started at 9 am after an overnight fast. The patient was kept on fluid restriction until 8 pm. Urine was collected every 2 hours and blood was drawn every 4 hours. At 5 pm, 2 µg desmopressin were injected intravenously. Urine was collected after another hour and the final pair of urine and serum samples was obtained at 8 pm. The second water deprivation test was started at 11 am with a continuous infusion of KCl that was titrated to raise serum K^+ by about 1 mmol/l throughout the test period. For this to occur, about 15 mmol KCl needed to be administered per hour. Serum K^+ levels and acid-base status were assessed every hour. Otherwise, the procedure did not differ from the first test.

The hypertonic saline infusion test for the assessment of hypertonic saline-stimulated serum copeptin was essentially performed as previously described.[6] The patient was asked to maintain a recumbent position for at least 30 min before the start of the procedure. The test was started at 9 am after an overnight fast. After initial blood sampling, 3% saline was administered as bolus (250 ml/ 15 min) before being continued at 0.15 ml/kg/min. Venous blood gas analyses were performed every 30 min. The procedure was stopped and the final blood sample was collected when venous Na^+ levels were ≥ 147 mmol/l on blood gas analysis. During saline infusion, vital parameters were monitored. After the test, the patient was asked to drink plenty of water (2-2.5 l in 30 min), before a 5% glucose infusion was installed (500 ml in 45-60 min), followed by final assessment of venous Na^+. Copeptin was measured in initial and final serum samples.

Further clinical tests

Salivation was stimulated by chewing a paraffin pellet (Ivoclar Vivadent, Liechtenstein) and stimulated saliva flow rates were assessed by collecting saliva over a period of 5 min after an initiation period of 1 min where the saliva produced was discarded. Subjects refrained from eating, drinking, consuming chewing gums, smoking, brushing of teeth, or using mouthwashes for at least one hour before the test.

Electrolyte concentrations in salivary fluid were measured on a Roche/ Hitachi cobas 8000 system, employing the serum/ plasma mode of the ion selective electrode module. For verification of data reliability, 2-3 independent samples were obtained for each subject.

For quantitative assessment of sweat secretion, sweat from several body parts (both axillae, palmar aspects of hands, plantar aspects of feet) was collected on filter paper and weighed before and after predefined exercise. Sweat collection periods were 1 min.

Schirmer's tests were performed without local anesthesia.

CLDN10 expression constructs

Site-directed mutagenesis was performed on human claudin-10a and claudin-10b cDNA sequences (c.488G>C in claudin-10a cDNA (NM_182848.3) and c.494G>C in claudin-10b cDNA (NM_006984.4), respectively) in pcDNA3-NECFP/-NEYFP vectors[7] using the Q5 Site-Directed Mutagenesis Kit (#E0554S, New England Biolabs, USA). Mutagenic primers were 5` GCTCTGTTTATTGCATGGGCAGGAGCCTC 3` (sense) and 5` GGCTCCTAATTCATACTTTTGCTCAACAAA GAGAG 3` (antisense). Successful mutagenesis was verified by Sanger sequencing. These N-terminally ECFP or EYFP tagged constructs were used for transient or stable expression in HEK293 cells. In this article, we refer to ECFP as CFP and to EYFP as YFP.

For transfection in MDCK-C7 cells, mutant human claudin-10a or claudin-10b cDNA inserts were cloned from pcDNA3-NECFP/-NEYFP vectors into a pCI-puro vector. To this end, the inserts were digested using SpeI and EagI restriction enzymes, and the pCI-puro vector was digested by NheI and

NotI enzymes. Wild-type human claudin-10a and claudin-10b cDNA sequences in pCI-puro vectors have previously been used.[8]

Immunofluorescence

Immunofluorescence labeling of tight junction components was performed on paraffin embedded human mucosal and skin samples as well as on MDCK-C7 cells stably transfected with untagged claudin-10 constructs. For paraffin-embedded samples, after deparaffination and hydration, antigens were retrieved by microwaving in TEC buffer (330 W, 30 min) and trypsination (0.001% in TEC buffer, 37°C, 10 min). Stably transfected MDCK-C7 cells were seeded in Nunc Lab-Tek II Chamber Slides (#154534, Thermo Scientific, USA). On day 6, cells were washed in PBS, fixed in 2% PFA in PBS, and permeabilized in 0.5% Triton X-100 in PBS. All tissue samples were blocked (4% goat serum in PBS) and incubated overnight at 4°C with primary antibodies diluted in blocking solution (1:100). Cultured cells were incubated overnight at 4°C with primary antibodies diluted in 0.1% Triton X-100 in PBS (1:100) without prior blocking. Incubation with secondary antibodies was done at room temperature for at least 45 min. Nuclei were stained with DAPI (#10236276001, Roche, Germany). All samples were covered with embedding media (ProTaqs MountFluor, #401603099, quartett, Germany). Fluorescence images were recorded with an LSM 780 system (Carl Zeiss Microscopy, Germany).

Primary antibodies: rabbit anti-claudin-10 (#38-8400, Invitrogen, USA), mouse anti-occludin (#33-1500, Invitrogen, USA), mouse anti-ZO-1 (#610966, BD Transduction Laboratories, USA), mouse anti-claudin-4 (#32-9400, Invitrogen, USA).

Secondary antibodies: Cy2 goat anti-mouse (#115-225-146, Jackson ImmunoResearch, UK), Cy5 goat anti-rabbit (#111-175-144, Jackson ImmunoResearch, UK), Cy2 goat anti-rabbit (#111-225-144, Jackson ImmunoResearch, UK), Cy5 goat anti-mouse (#115-175-146, Jackson ImmunoResearch, UK), Alexa Fluor 594 goat anti-rabbit (#A-11037, Invitrogen, USA), Alexa Fluor Plus 488 goat anti-rabbit (A32731, Invitrogen, USA), Alexa Fluor Plus 594 goat anti-mouse (#A32742, Invitrogen, USA).

Quantification of tight junctional claudin-10b WT and G165A in stably transfected MDCK-C7 cells:

The Zeiss ZEN black software was used to set an intensity threshold of 50 (on a scale of 256 grey values) to determine the number of pixels and mean intensities for non-tight junctional claudin-10 (claudin-10 signal >50, occludin signal <50) and tight junctional claudin-10 (claudin-10 signal >50, occludin signal >50). The relative amount of tight junctional claudin-10 was then calculated as

$$\frac{(number\ of\ pixels\ \times mean\ intensity)_{TJ\ claudin-10}}{(number\ of\ pixels\ \times mean\ intensity)_{TJ\ claudin-10} + (number\ of\ pixels\ \times mean\ intensity)_{non-TJ\ claudin-10}} \times 100\%.$$

For each MDCK-C7 clone included in this analysis, ten images (two seedings with five images taken from each) were assessed.

Immunohistochemistry

Immunohistochemical staining of claudin-10 was performed on paraffin embedded human skin samples using a labeled streptavidin/ biotin detection system (#K5005, Dako, Denmark). After deparaffination and hydration, heat-induced epitope retrieval (97-99°C, 15 min) in Tris/EDTA buffer followed (1:10, #K8004, Dako, Denmark), before inhibition of endogenous alkaline phosphatase activity (#S2003, Dako, Denmark). Samples were incubated with primary antibody (rabbit anti-claudin-10, #38-8400, Invitrogen, USA) diluted at 1:200 (#S3022, Dako, Denmark) for 30 min, followed by incubation with biotinylated secondary antibody for 20 min. Samples were incubated with alkaline phosphatase-conjugated streptavidin for 20 min before incubation with the chromogen substrate for 10-15 min. Between individual steps, specimens were washed twice with TBS. The staining procedure was done at room temperature. Hematoxylin counterstaining was performed.

Structural bioinformatics and molecular modeling

Homology models were created utilizing MODELLER[9] and Schrödinger's BioLuminate/ Maestro (Biologics Suite, Release 2019-2, Schrödinger, Germany). For the claudin-10b protomer model, the claudin-15 crystal structure[10] (PDB ID 4P79) was used as template. For the claudin-10a protomer model, the claudin-10b model was used as template. For claudin-10b, the human sequence 1-186 was used and the β1β2 loop that misses in the claudin-15 template was modeled *ab initio*. For

claudin-10a, the human sequence 1-184 was used. All manual manipulations and optimizations were performed with Schrödinger's BioLuminate/ Maestro (Biologics Suite, Release 2019-2, Schrödinger, Germany). Images were created with PyMOL 2.3 (Schrödinger, Germany).

Cell culture and transfection before the assessment of claudin-10 trans*-interaction*

HEK293 cells (#ACC 305, Leibniz Institute DSMZ - German Collection of Microorganisms and Cell Cultures, Germany) were cultured in a 1:1 mixture of Dulbecco`s Modified Eagle Medium and Ham`s F-12 nutrient mixture (#11320074, Gibco, UK) supplemented with 15% (v/v) fetal bovine serum at 37°C in a humidified 5% CO_2 atmosphere. Cells were seeded in chambered slides (#80826 with ibiTreat surface, ibidi, Germany) and transfected on the following day using Lipofectamine 2000 (#11668019, Invitrogen, USA). For staining of acidic organelles, cells were incubated in 1:15,000 diluted LysoTracker Red DND-99 (#L7528, Invitrogen, USA) for 60 min prior to live cell imaging. After fixation, nuclei were stained with DAPI (#R37606, Invitrogen, USA) before the samples were subjected to imaging. On a single given chambered slide, eight mutually different experiments were run. Each experiment was performed three times. Images were acquired at an Axio Observer.Z1 microscope with an ApoTome.2 imaging system (Carl Zeiss Microscopy, Germany). Exposure times were identical for all images reported. Image processing was performed with ZEN 2 software (Carl Zeiss Microscopy, Germany).

For quantification of claudin-10 enrichment at cell-cell contacts, enrichment factors were calculated essentially as previously described.[11] For a given cell-cell contact between two claudin-10 expressing cells a and b, the enrichment factor EnF was computed from triplicate measurements of fluorescence intensity at the cell-cell contact as well as at cell membrane segments of either cell without contact to a claudin-10 expressing cell:

$$EnF = \frac{I_C}{I_{M,a} + I_{M,b}}$$

with I_C, sum of triplicate measurements of fluorescence intensity at cell-cell contact, and $I_{M,x}$, sum of triplicate measurements of fluorescence intensity at membrane of cell x without contact to a claudin-10 expressing cell. EnF > 1 indicates *trans*-interaction.

Cell culture and transfection before Förster resonance energy transfer (FRET) studies, freeze-fracture electron microscopy, and immunofluorescence staining

MDCK-C7 cells and HEK293 cells were cultured in MEM-Earle's media (Sigma-Aldrich, Germany) supplemented with 10% (v/v) fetal bovine serum, 100 U/ml penicillin, and 100 µg/ml streptomycin (Sigma-Aldrich, Germany) at 37°C in a humidified 5% CO_2 atmosphere. Cell lines were transfected using Lipofectamine 2000 (MDCK-C7, Invitrogen, USA) or polyethylenimine (HEK293, Polysciences, USA) according to the manufacturer's recommendations 24 h post seeding. For stable MDCK-C7 cell lines, transfectants were selected with 10 µg/ml puromycin for 7 days and maintained as clonal or polyclonal cell lines with 1 µg/ml puromycin. For stable HEK293 cell lines, transfectants were selected using 1000 U/mL G418-BC (Biochrom, Germany) and maintained as clonal or polyclonal cell lines with 600 U/mL G418-BC.

FRET assay

FRET was assessed between CFP- and YFP-claudin fusion proteins in HEK293 cells essentially as previously described.[11] For transient coexpression of CFP and YFP tagged claudins, HEK293 cells were seeded on Poly-L-Lysine coated glass coverslips and transfected one day later with polyethylenimine (Polysciences, USA). 1-2 days after transfection, cells were transferred to a HEPES buffered solution (134.6 mM NaCl, 2.4 mM Na_2HPO_4, 0.6 mM NaH_2PO_4, 5.4 mM KCl, 1.2 mM $CaCl_2$, 1 mM $MgSO_4$, 10 mM HEPES, 10 mM D(+)-glucose, pH 7.4) before live-cell imaging on a LSM 780 system (Carl Zeiss Microscopy, Germany).

The FRET efficiency E_F was computed from the increase in CFP fluorescence intensity after FRET acceptor (YFP) photobleaching:

$$E_F = \frac{(I_a - I_b)}{I_a}$$

with I_a, CFP fluorescence intensity after acceptor bleaching, and I_b, CFP fluorescence intensity before acceptor bleaching.

Experiments were carried out at different YFP/CFP ratios. E_F values were plotted against the corresponding YFP/CFP ratios. Because of the strong dependence of E_F on the YFP/CFP ratio, for statistical comparisons, data points were selected according to their YFP/CFP ratios to obtain data sets with comparable FRET acceptor/donor ratios (i.e., YFP/CFP ratios not significantly different from one another, two-tailed t-tests performed in Microsoft Excel 2016 (Microsoft, USA)).

Freeze-fracture electron microscopy

Stably transfected HEK293 cells were grown in six well plates until confluency and processed for freeze-fracture electron microscopy as previously reported.[7] For quantification of strand breaks, electron micrographs were analyzed using Image J. First, the total length of strands in a given tight junction meshwork was measured. Next, the sum of gaps (> 5 nm) between strand segments or particles was determined. The break percentage was then calculated from the quotient of total gap length and total strand length.

Electrophysiology

Dilution and biionic potential measurements were essentially carried out as previously described.[12] Stably transfected MDCK-C7 cells were seeded on culture plate inserts (pore size 0.4 µm, effective area 0.6 cm^2; Millicell-PCF, Merck, Germany). Confluent cell layers were used on days 5-7 after seeding. Inserts were mounted in Ussing chambers specially designed for insertion of Millicell filters,[13] and water-jacketed gas lifts were filled with 10 ml circulating fluid on each side. The standard bath solution contained 119 mM NaCl, 21 mM $NaHCO_3$, 5.4 mM KCl, 1.2 mM $CaCl_2$, 1 mM $MgSO_4$, 3 mM Hepes, and 10 mM D(+)-glucose. The solution was constantly bubbled with 95% O_2 and 5% CO_2 to ensure a pH of 7.4 at 37°C.

Transepithelial resistance was assessed every 10 s and corrected for the resistance of bath solution and filter support. To determine relative ion permeabilities, 5 ml of the standard bath solution on either the apical or the basolateral side of the cell layer was replaced by a solution in which NaCl was isoosmotically replaced by mannitol (dilution potential measurements to determine P_{Na}/P_{Cl}), or by LiCl, KCl, RbCl, or CsCl, respectively (biionic potential measurements to determine Eisenman sequences of the paracellular pathway), or by NH_4Cl (unhydrated NH_4^+ ion diameter[14] 2.96 Å), MA chloride (methylammonium, ion diameter d = 3.76 Å), DMA chloride (dimethylammonium, d = 4.60 Å), TriMA chloride (trimethylammonium, d = 5.06 Å), or TeMA chloride (tetramethylammonium, d = 5.5 Å), respectively (biionic potential measurements to determine the pore diameter of the paracellular pathway). If not referenced otherwise, ion diameters were calculated as geometric means from dimensions given by Villarroel et al.[15] All resulting potential differences were corrected for liquid junction potentials. These were determined as previously described.[16]

P_{Na}/P_{Cl} was calculated from corrected potential differences, ΔE^{corr}, using the simplified Goldman-Hodgkin-Katz equation

$$\frac{P_{Na}}{P_{Cl}} = \frac{10^{\left(\frac{\Delta E^{corr}}{s}\right)} \cdot [Cl^-]_{ap} - [Cl^-]_{bl}}{[Na^+]_{ap} - 10^{\left(\frac{\Delta E^{corr}}{s}\right)} \cdot [Na^+]_{bl}}$$

with $s = ln(10) \cdot R \cdot T/F$ (R, universal gas constant; T, absolute temperature; F, Faraday constant). Here, ap denotes the apical side and bl the basolateral side of the cell layer.

Relative permeabilities P_X/P_{Na} for all cations X^+ were calculated using the modified Goldman-Hodgkin-Katz equation

$$\frac{P_X}{P_{Na}} = \frac{[Na^+]_{ap} + \frac{P_{Cl}}{P_{Na}} \cdot [Cl^-]_{bl} - 10^{(\Delta E^{corr}/s)} \cdot \left([Na^+]_{bl} + \frac{P_{Cl}}{P_{Na}} \cdot [Cl^-]_{ap}\right)}{10^{(\Delta E^{corr}/s)} \cdot [X^+]_{bl} - [X^+]_{ap}}$$

with s as defined above.

Here, P_{Na}/P_{Cl} was determined within the same experiment for each cell layer.

Pore diameter was estimated by plotting the square root of P_X/P_{Na} (X, NH_4^+ and various organic cations) against cation diameters and extrapolating the linear part of the relationship.[16]

Statistics

Statistical methods were employed as indicated. Statistical significance was assumed at $p<0.05$. Quantitative data from the assessment of claudin enrichment at cell-cell contacts in HEK293 cells were analyzed by means of Welch's one-way ANOVA with Dunnett's T3 multiple comparisons test using GraphPad Prism 9.1.0.221 software (GraphPad Software, USA) (**Fig. 5B**). FRET efficiencies were analyzed separately for claudin-10a and -10b by means of ordinary one-way ANOVAs using GraphPad Prism 9.1.0.221 software (GraphPad Software, USA) followed by two-tailed t-tests with Bonferroni-Holm correction using Microsoft Excel 2016 (Microsoft, USA) (**Fig. 5C**). Data sets for comparison of FRET efficiencies were obtained as detailed above. Quantitative data from electron micrographs were analyzed with a Kruskal-Wallis test followed by post-hoc two-tailed Mann Whitney tests with Holm-Šídák multiple comparisons test using GraphPad Prism 7.04 software (GraphPad Software, USA) (**Fig. 6H**). Quantitative data on the amount of claudin-10b at tight junctions in stably transfected MDCK-C7 cells were analyzed by means of a Kruskal-Wallis test with Dunn's multiple comparisons test using GraphPad Prism 9.1.0.221 software (GraphPad Software, USA) (**Fig. S6**). In electrophysiological studies on stably transfected MDCK-C7 cells, $\sqrt{(P_X/P_{Na})}$ values with X representing NH_4^+ or MA were compared by means of two-tailed t-tests using GraphPad Prism 9.1.0.221 software (GraphPad Software, USA) (**Fig. 7F**).

Table S1

Laboratory test results from the patient at initial presentation.

	Reference range	Patient test results
Whole blood		
Na^+ [mmol/l]	134 – 143	137.0
K^+ [mmol/l]	3.49 – 4.63	2.70
Cl^- [mmol/l]	96 – 111	88.0
Ca^{2+}, ionized [mmol/l]	1.15 – 1.35	1.18
Serum		
Mg^{2+} [mmol/l]	0.7 – 0.91	1.04[a]
Creatinine [µmol/l]	59 – 104	79.0
Urea [mmol/l]	< 8	5.90
Aldosterone [pmol/l]		856.0
Renin [mU/l]	2.8 – 39.9	531.0
Venous blood gas analysis		
pH []	7.35 – 7.43	7.486
pCO_2 [mmHg]	37 – 50	50.80
pO_2 [mmHg]	36 – 44	49.70
Standard HCO_3^- [mmol/l]	21 – 26	36.0
Actual HCO_3^- [mmol/l]	21 – 26	37.9
Base excess [mmol/l]	-2 – 3	13.5
Urine (spot sample)		
pH []	5.0 – 7.5	ca. 6.0[b]
Na^+ [mmol/l]	54 – 190	26.8
K^+ [mmol/l]	20 – 80	28.2
Cl^- [mmol/l]	46 – 199	27.0
Ca^{2+} [mmol/l]		0.48
Ca^{2+}/ Creatinine [mmol/mmol]		0.02
Mg^{2+} [mmol/l]		1.86[a]

[a] not first available value, but representative in nature; [b] from urine dipstick analysis

Supplementary Information on Figure 4

(**B**) G165 is in close proximity to a number of positions (yellow sticks and labels) that have been implicated in claudin structure and function. For claudin-5, the residues corresponding to A161 and I164 of claudin-10b have been shown to be involved in claudin assembly.[17] In claudin-14, the substitution A163V at the position corresponding to A161 in claudin-10b causes hearing loss.[18] In claudin-2, the substitution G161R whose position corresponds to that of G159 in claudin-10b is associated with obstructive azoospermia[19] as well as hypercalciuria and nephrolithiasis.[20] G134 of claudin-10b corresponds to P134 in claudin-3 which has been shown to be involved in the bending of transmembrane helix 3 that was suggested to influence claudin *cis*-interaction.[21]

Furthermore, the residue S131 (red stick) whose exchange for leucine (S131L) in claudin-10b causes HELIX syndrome,[22] is located right beneath C133 which is close to G165. In contrast, other HELIX syndrome causing mutations involve positions further away from G165 (N48K, Klar et al. 2017;[8] D73N, P149R, Bongers et al. 2017;[23] R80G, Meyers et al. 2019;[24] the corresponding residues are shown as red sticks).

(**C-F**) Hydrogen bonding between the hydroxyl group of T24 and the backbone carbonyl group of L20 in claudin-10b might entail an intra-helical hydrogen bond pattern different from that in claudin-10a where A22 does not provide a hydroxyl group. As a consequence, G163A/G165A may perturb the four-helix bundle of claudin-10b slightly more severely than that of claudin-10a.

References

1. Lu H, Galeano MCR, Ott E, et al. Mutations in *DZIP1L*, which encodes a ciliary-transition-zone protein, cause autosomal recessive polycystic kidney disease. *Nat Genet*. 2017;49(7):1025-1034.
2. Colussi G, Bettinelli A, Tedeschi S, et al. A thiazide test for the diagnosis of renal tubular hypokalemic disorders. *Clin J Am Soc Nephrol*. 2007;2(3):454-460.

3. Tsukamoto T, Kobayashi T, Kawamoto K, Fukase M, Chihara K. Possible discrimination of Gitelman's syndrome from Bartter's syndrome by renal clearance study: report of two cases. *Am J Kidney Dis*. 1995;25(4):637-641.
4. Nozu K, Iijima K, Kanda K, et al. The pharmacological characteristics of molecular-based inherited salt-losing tubulopathies. *J Clin Endocrinol Metab*. 2010;95(12):E511-E518.
5. Viering DHHM, Baaij JHF de, Walsh SB, Kleta R, Bockenhauer D. Genetic causes of hypomagnesemia, a clinical overview. *Pediatr Nephrol*. 2017;32(7):1123-1135.
6. Fenske W, Refardt J, Chifu I, et al. A copeptin-based approach in the diagnosis of diabetes insipidus. *N Engl J Med*. 2018;379(5):428-439.
7. Milatz S, Piontek J, Hempel C, et al. Tight junction strand formation by claudin-10 isoforms and claudin-10a/-10b chimeras. *Ann N Y Acad Sci*. 2017;1405(1):102-115.
8. Klar J, Piontek J, Milatz S, et al. Altered paracellular cation permeability due to a rare *CLDN10B* variant causes anhidrosis and kidney damage. *PLoS Genet*. 2017;13(7), e1006897.
9. Fiser A, Šali A. Modeller: generation and refinement of homology-based protein structure models. In: Carter Jr CW, Sweet RM, eds. *Methods in Enzymology: Macromolecular Crystallography, Part D*. Vol. 374. New York, NY: Academic Press; 2003:461-491.
10. Suzuki H, Nishizawa T, Tani K, et al. Crystal structure of a claudin provides insight into the architecture of tight junctions. *Science*. 2014;344(6181):304-307.
11. Milatz S, Piontek J, Schulzke J-D, Blasig IE, Fromm M, Günzel D. Probing the *cis*-arrangement of prototype tight junction proteins claudin-1 and claudin-3. *Biochem J*. 2015;468(3):449-458.
12. Günzel D, Stuiver M, Kausalya PJ, et al. Claudin-10 exists in six alternatively spliced isoforms that exhibit distinct localization and function. *J Cell Sci*. 2009;122(10):1507-1517.
13. Kreusel K-M, Fromm M, Schulzke J-D, Hegel U. Cl^- secretion in epithelial monolayers of mucus-forming human colon cells (HT-29/B6). *Am J Physiol Cell Physiol*. 1991;261(4):C574-C582.
14. Nightingale ER. Phenomenological theory of ion solvation. Effective radii of hydrated ions. *J Phys Chem*. 1959;63(9):1381-1387.

15. Villarroel A, Burnashev N, Sakmann B. Dimensions of the narrow portion of a recombinant NMDA receptor channel. *Biophys J*. 1995;68(3):866-875.
16. Yu ASL, Cheng MH, Angelow S, et al. Molecular basis for cation selectivity in claudin-2-based paracellular pores: identification of an electrostatic interaction site. *J Gen Physiol*. 2009;133(1):111-127.
17. Rossa J, Protze J, Kern C, et al. Molecular and structural transmembrane determinants critical for embedding claudin-5 into tight junctions reveal a distinct four-helix bundle arrangement. *Biochem J*. 2014;464(1):49-60.
18. Pater JA, Benteau T, Griffin A, et al. A common variant in *CLDN14* causes precipitous, prelingual sensorineural hearing loss in multiple families due to founder effect. *Hum Genet*. 2017;136(1):107-118.
19. Askari M, Karamzadeh R, Ansari-Pour N, et al. Identification of a missense variant in *CLDN2* in obstructive azoospermia. *J Hum Genet*. 2019;64(10):1023-1032.
20. Curry JN, Saurette M, Askari M, et al. Claudin-2 deficiency associates with hypercalciuria in mice and human kidney stone disease. *J Clin Invest*. 2020;130(4):1948-1960.
21. Nakamura S, Irie K, Tanaka H, et al. Morphologic determinant of tight junctions revealed by claudin-3 structures. *Nat Commun*. 2019;10(1), e816.
22. Hadj-Rabia S, Brideau G, Al-Sarraj Y, et al. Multiplex epithelium dysfunction due to *CLDN10* mutation: the HELIX syndrome. *Genet Med*. 2018;20(2):190-201.
23. Bongers EMHF, Shelton LM, Milatz S, et al. A novel hypokalemic-alkalotic salt-losing tubulopathy in patients with *CLDN10* mutations. *J Am Soc Nephrol*. 2017;28(10):3118-3128.
24. Meyers N, Nelson-Williams C, Malaga-Dieguez L, et al. Hypokalemia associated with a claudin 10 mutation: a case report. *Am J Kidney Dis*. 2019;73(3):425-428.

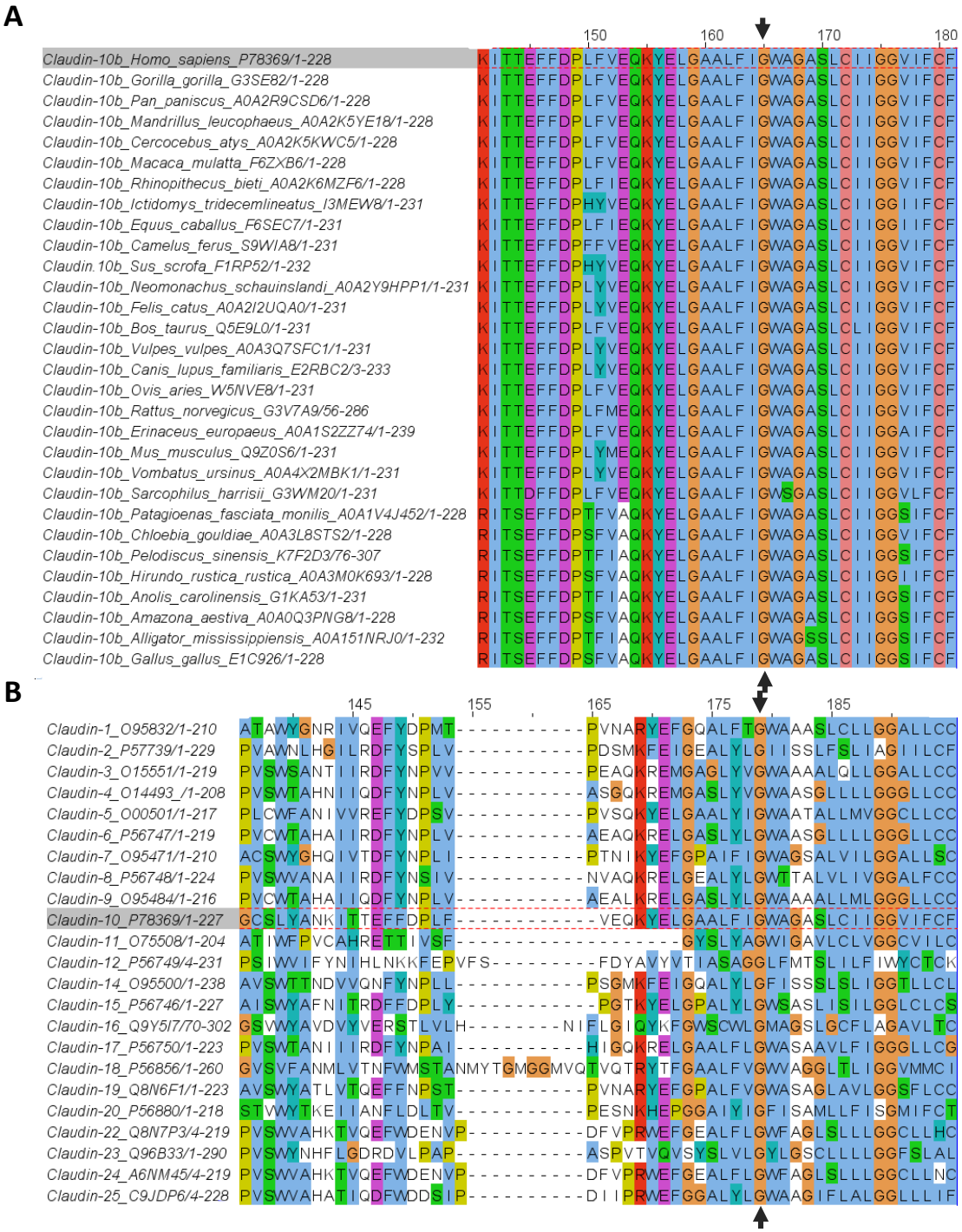

Figure S1. G165 of claudin-10b is highly conserved across species and among claudin family members. (**A**) Alignment of claudin-10b amino acid sequences from different species, demonstrating 100% conservation of G165 (arrows). 30 sequences showing higher homology along the full coding sequence than the human claudin-10 isoforms a and b were selected for the alignment. Uniprot/EMBL-EBI accession numbers are given behind the species' names. Numbering according to the human claudin-10b positions. A relevant part of the sequence alignment is depicted. Color code for amino acids: red, positive; magenta, negative; green, polar; cyan, hydrophobic; orange, Gly; white, Ala; pink, Cys. (**B**) Alignment of amino acid sequences from human claudin family members. The glycine residue (arrows) corresponding to G163 in claudin-10a and G165 in claudin-10b is 100% conserved among human claudin family members. Uniprot/EMBL-EBI accession numbers are given behind the claudin names. Numbering according to the alignment. A relevant part of the sequence alignment is depicted. Color code for amino acids: red, positive; magenta, negative; green, polar; cyan, hydrophobic and Cys; orange, Gly; white, some unassigned residues. Alignments were generated with Clustal Omega and visualized with Jalview.

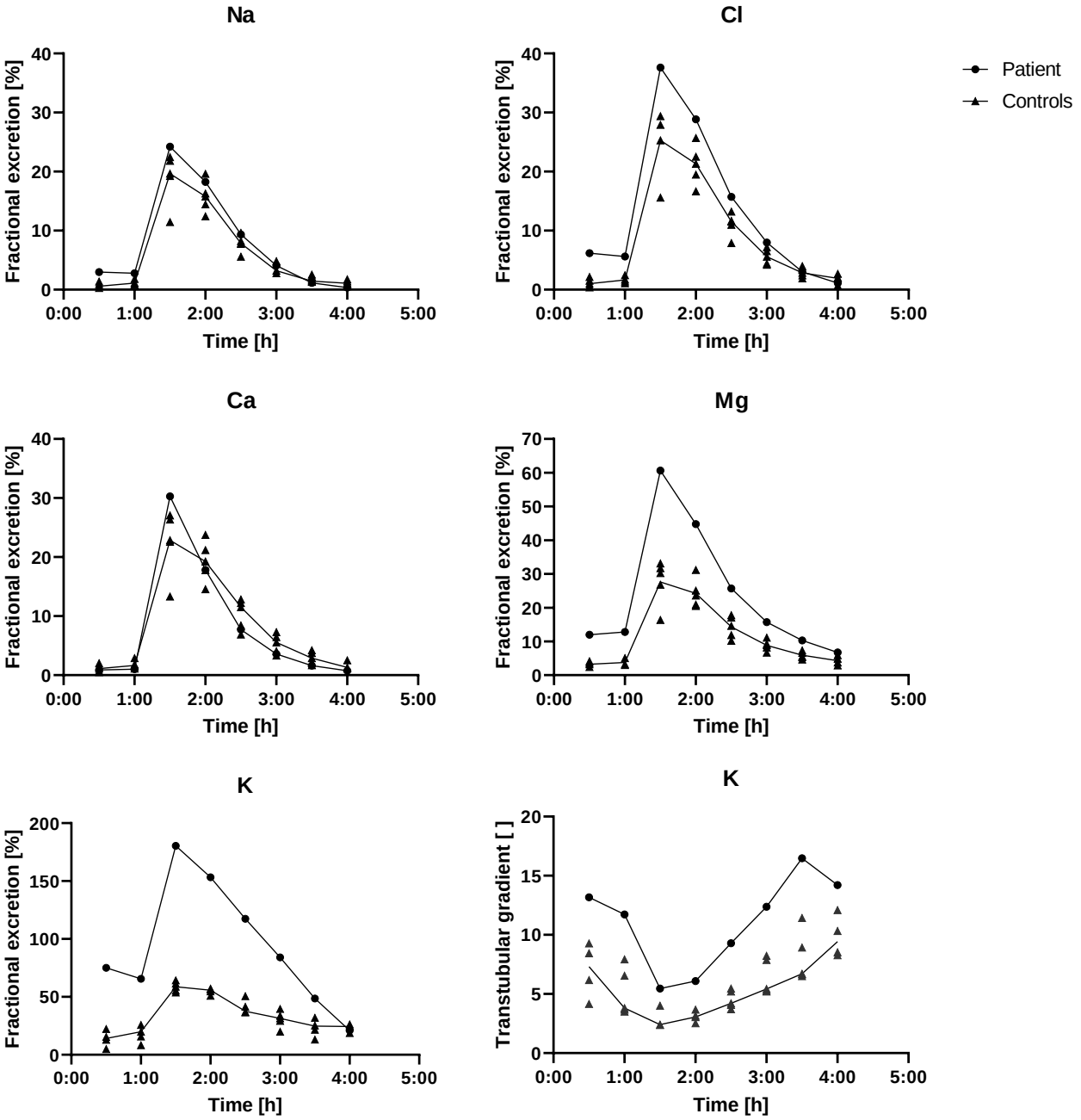

Figure S2. Furosemide responsiveness testing in the patient and in 5 control subjects. The loop diuretic was administered intravenously at t=1:00 h. Shown are fractional excretions for Na^+, Cl^-, K^+, Ca^{2+}, and Mg^{2+} as well as the transtubular K^+ concentration gradient (TTKG) over time. Note the high baseline fractional K^+ excretion and TTKG values in the patient, signifying high basal activity of the distal nephron K^+ secretory process. We propose that loop diuretic induced reductions of TTKG result from an increased volume load in nephron segments downstream from the thick ascending limb of Henle's loop (TAL). Assuming complete abolishment of TAL paracellular Na^+ transport due to claudin-10 deficiency, the preserved or even slightly increased response of fractional Na^+ and Cl^- excretions to furosemide is compatible with adaptive upregulation of TAL transcellular Na^+ transport: At submaximal loop diuretic doses, there would be residual paracellular Na^+ transport in controls, while the absolute loop diuretic effect on transcellular Na^+ transport would be greater in the patient. Note that compensation by an increase in TAL transcellular Na^+ transport has to be partial for otherwise there would be no defect in urinary concentration ability. Medians connected.

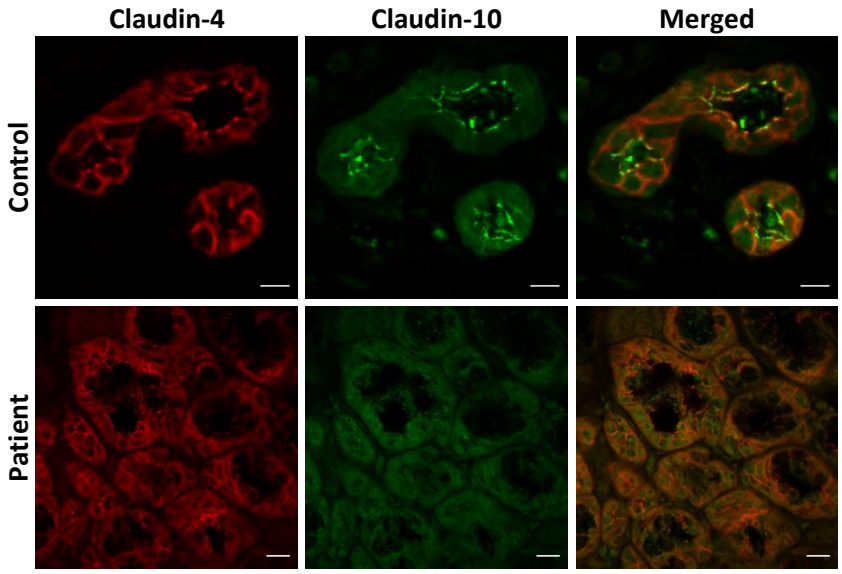

Figure S3. Immunofluorescence labeling of claudin-10 and claudin-4 in submucosal salivary glands from the labial mucosa. When compared with control tissue, a complete absence of claudin-10 in the presence of a preserved claudin-4 signal is evident in the patient. Scale bars, 10 µm (upper row) or 20 µm (lower row).

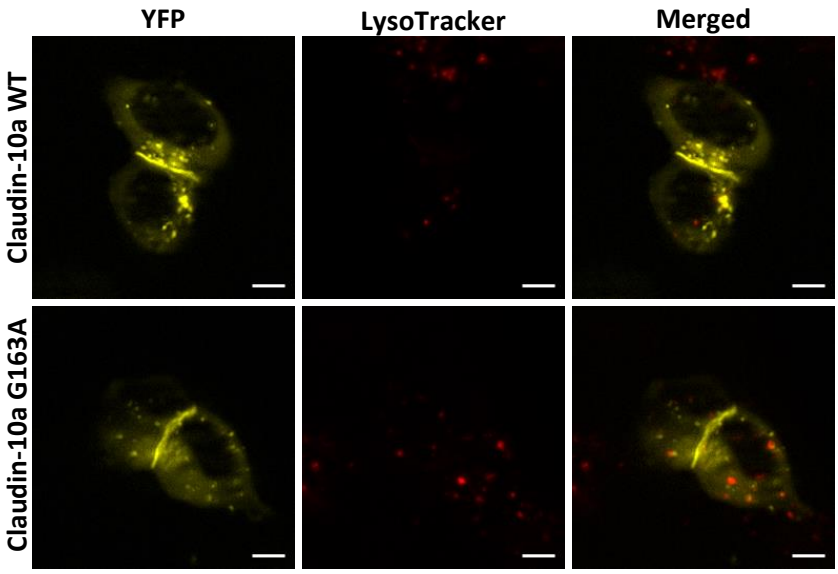

Figure S4. Live cell imaging of HEK293 cells transiently expressing YFP tagged claudin-10a WT or G163A demonstrates that claudin-10a localizes to non-acidic intracellular granules. The YFP signal does not colocalize with lysosomes as indicated by fluorescence labeling. Scale bars, 5 µm. WT, wild-type.

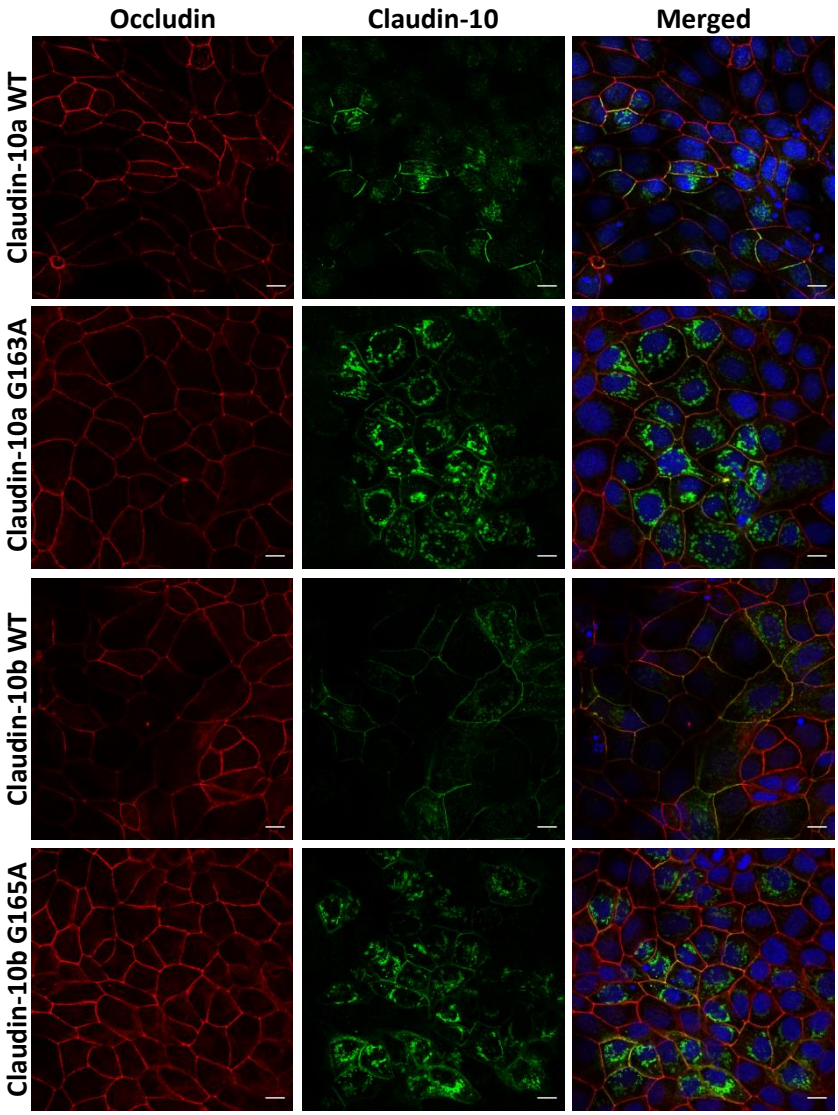

Figure S5. Immunofluorescence labeling of exogenous claudin-10 in MDCK-C7 cells demonstrates pronounced intracellular accumulation of mutant proteins. MDCK-C7 cells were stably transfected with wild-type or mutant claudin-10 constructs. All claudin-10 proteins localize to the plasma membrane. In addition, both claudin-10a G163A and claudin-10b G165A show perinuclear accumulation in a mottled pattern. These effects are markedly less pronounced in claudin-10a/b WT expressing cells. Nuclei are stained with DAPI (blue). Scale bars, 10 µm. WT, wild-type.

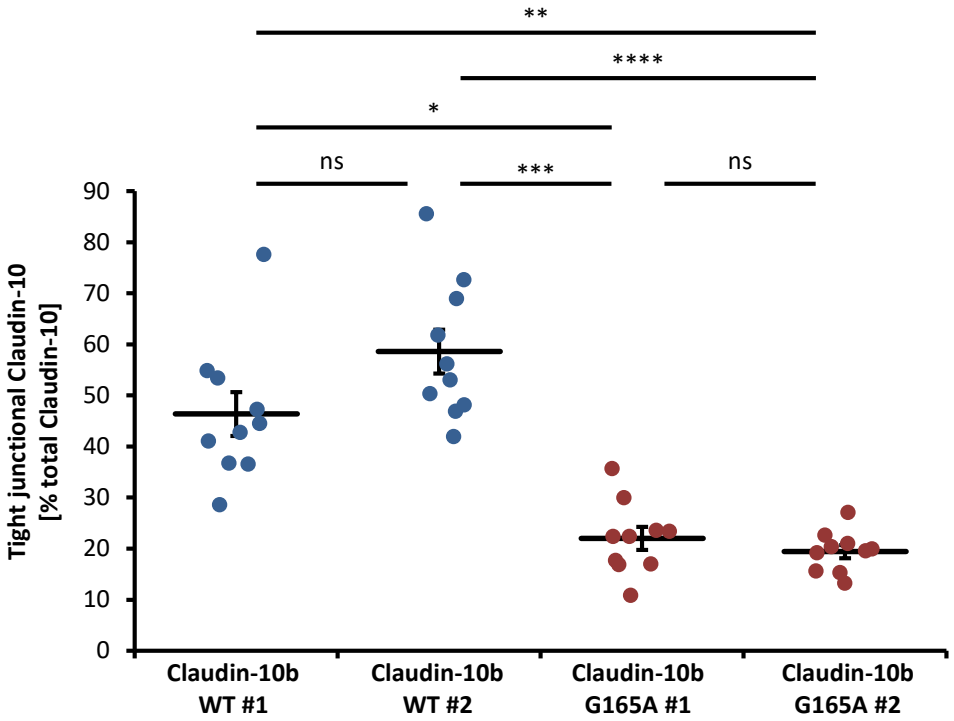

Figure S6. Quantification of exogenous claudin-10b WT and G165A in MDCK-C7 cells demonstrates reduced relative amounts of tight junctional claudin-10b in the mutant case. MDCK-C7 cells were stably transfected with wild-type or mutant claudin-10b constructs. For both claudin-10b WT and G165A, data from two different stably transfected clones (#) are shown. Kruskal-Wallis test with Dunn's multiple comparisons test; ns, not significant; *, $p<0.05$; **, $p<0.01$; ***, $p<0.001$; ****, $p<0.0001$. Mean ± SEM. WT, wild-type.